Results in Chemistry 32 (2026) 104057

Contents lists available at ScienceDirect

Results in Chemistry

journal homepage: www.sciencedirect.com/journal/results-in-chemistry

# Design, synthesis, and biological evaluation of novel 4-(3-(4-fluorophenoxy) azetidin-1-yl) pyridazin-3(2*H*)-one derivatives against interleukin-2-inducible T-cell kinase and Bruton's tyrosine kinase

Sudhakar Tangallapalli [a,b], Rambabu Gundla [a,*], Kalyani Paidikondala [a], Naveen Kumar Rampeesa [b], Sreenivasa Reddy Anugu [b], Soňa Gurská [c,d], Petr Džubák [c,d], Marián Hajdúch [c,d], Viswanath Das [c,d,**], Naresh Kumar Katari [e,f,***]

[a] *Department of Chemistry, School of Science, GITAM University, Hyderabad 502102, Telangana, India*
[b] *Aragen Life Sciences Ltd, Medicinal Chemistry Laboratory Division, Survey No: 125(Part) & 126, IDA Mallapur, Hyderabad 500076, India*
[c] *Institute of Molecular and Translational Medicine, Faculty of Medicine and Dentistry, Palacký University and University Hospital Olomouc, Hněvotínská 1333/5, 779 00 Olomouc, Czech Republic*
[d] *Institute of Molecular and Translational Medicine, Czech Advanced Technologies and Research Institute, Palacký University Olomouc, Křížkovského 511/8, 779 00 Olomouc, Czech Republic*
[e] *School of Chemistry & Physics, College of Agriculture, Engineering & Science, Westville Campus, University of KwaZulu-Natal, P Bag X 54001, Durban 4000, South Africa*
[f] *A&B Laboratories (an AmSpec Group of Company), 10100 East Freeway, Suite 100, Houston, TX 77029, USA*

ARTICLE INFO

*Keywords:*
Azetidine
BTK
Cell viability
ITK
Kinase activity
Molecular docking
Pyridazin-3(2H)-one

ABSTRACT

Ten 4-(3-(4-fluorophenoxy)azetidin-1-yl)pyridazin-3(2*H*)-one derivatives **(7a–7j)** were synthesized and characterized. Their effects on cell viability were evaluated in a panel comprising reported interleukin-2-inducible T-cell kinase (ITK)-expressing T-cell leukemia lines (Jurkat and CCRF-CEM), reported Bruton's tyrosine kinase (BTK)-expressing hematological lines (Ramos and K562), cancer cell lines not reported to express either kinase, and non-cancer fibroblasts. Compound **7a** was the most active analog, with $IC_{50}$ values of 19.23 ± 1.19 μM in Jurkat, 21.92 ± 2.47 μM in CCRF-CEM, and 22.59 ± 2.79 μM in Ramos cells, whereas most other analogs showed weak or no activity. Compounds **7a** and **7e**, the latter producing the most favorable predicted ITK docking score, were subsequently evaluated against recombinant ITK and BTK at 1, 10, and 20 μM, with ibrutinib included as a reference inhibitor. At 20 μM, **7a** reduced ITK and BTK activity to 58.7 ± 5.2% and 58.5 ± 3.6% of vehicle-control activity, respectively, demonstrating only partial inhibition without ITK selectivity. Compound **7e** did not inhibit either kinase. AutoDock Vina scores ranged from −8.5 to −7.5 kcal/mol, with **7e** producing the most favorable score despite its lack of biochemical activity. Thus, the docking ranking did not predict measured kinase inhibition. Overall, **7a** emerged as the most active analog, combining moderate activity in hematological cancer cell lines with partial inhibition of both ITK and BTK, and provides a promising starting point for further structural optimization.

## 1. Introduction

Interleukin-2-inducible T-cell kinase (ITK) is a Tec-family non-receptor tyrosine kinase expressed predominantly in T-lineage cells [1]. Following T-cell receptor activation, ITK is recruited to signaling complexes assembled around linker for activated T cells and SLP-76, where it promotes phosphorylation of phospholipase C-γ1 and downstream calcium mobilization, cytoskeletal reorganization, and transcriptional

* Corresponding author.
** Corresponding author at: Institute of Molecular and Translational Medicine, Faculty of Medicine and Dentistry, Palacký University and University Hospital Olomouc, Hněvotínská 1333/5, 779 00 Olomouc, Czech Republic.
*** Corresponding author at: School of Chemistry & Physics, College of Agriculture, Engineering & Science, Westville Campus, University of KwaZulu-Natal, P Bag X 54001, Durban 4000, South Africa.
*E-mail addresses:* rgundla@gitam.edu (R. Gundla), viswanath.das@upol.cz (V. Das), KatariN@ukzn.ac.za (N.K. Katari).

https://doi.org/10.1016/j.rechem.2026.104057
Received 22 August 2026; Accepted 8 November 2026
Available online 9 November 2026
2211-7156/© 2026 The Authors. Published by Elsevier B.V. This is an open access article under the CC BY license (http://creativecommons.org/licenses/by/4.0/).

responses [2]. Through these pathways, ITK contributes to T-cell development, activation, and differentiation [3].

ITK has been investigated as a pharmacological target in immune and inflammatory disorders and in selected T-cell malignancies. Its therapeutic interpretation is nevertheless context-dependent because ITK also regulates normal T-cell function and antitumor immunity [4]. Recent medicinal chemistry studies have continued to explore heterocyclic kinase inhibitors with anti-inflammatory and antiproliferative activities [5,6]. Moreover, ITK shares structural features with other Tec-family kinases, including Bruton's tyrosine kinase (BTK); ibrutinib, for example, inhibits both BTK and ITK [7]. Previous studies have reported pyridazine- and pyridazinone-containing scaffolds as potent BTK inhibitors, including pyrazolo[3,4-*d*]pyridazinone derivatives in which compound 8 showed potent BTK inhibition and in vivo efficacy [8], and pyridazinone analogues in which compound 23 displayed improved potency and metabolic stability [9]. More recently, imidazo[1,2-*b*]pyridazine derivatives have also been identified as potent and highly selective BTK inhibitors, with compound 22 showing an IC50 of 1.3 nM against BTK [10]. These studies highlight the potential of pyridazine-based heterocycles for Tec-family kinase inhibition. Direct biochemical testing against both kinases is therefore necessary before assigning ITK activity or selectivity. Cell-viability assays can identify a phenotype but cannot establish the responsible molecular target, while docking provides only a predicted binding hypothesis.

Pyridazinone derivatives provide a synthetically accessible heterocyclic scaffold for modern medicinal chemistry exploration. The pyridazinone ring system has attracted considerable interest due to its diverse biological functions, synthetic feasibility, and ability to form critical hydrogen-bonding interactions with catalytic residues [11]. Substituted pyridazin-3(2H)-ones provide an appealing framework for the design of kinase inhibitors due to their planar geometry, adjustable electronic properties, and suitability for various pharmacophoric alterations. Recent studies have further demonstrated the potential of pyridazinone scaffolds in kinase-directed anticancer research, including EGFRWT/EGFRT790M and dual EGFR/VEGFR-2 kinase inhibitors [5,12].

Building on our earlier study of 3-oxo-2,3-dihydropyridazine derivatives [13], we introduced a 4-fluorophenoxy-substituted azetidine unit at C-4 of the pyridazin-3(2H)-one core and varied the C-6 substituent to generate compounds **7a–7j** (Fig. 1). This series was designed to examine how these substitutions influence cellular activity and predicted accommodation within the ITK ATP-binding pocket. The synthesized compounds were characterized and evaluated in a 72 h cell viability panel. Compound **7a**, the most active cellular analog, and compound **7e**, which produced the most favorable ITK docking score, were then tested directly against recombinant ITK and BTK at three concentrations, using ibrutinib as a reference inhibitor. This combined design allowed the cellular and docking rankings to be compared with measured biochemical kinase activity without presuming an ITK-dependent mechanism.

## 2. Results

### 2.1. Chemistry

A series of 4-(3-(4-fluorophenoxy)azetidin-1-yl)pyridazin-3(2*H*)-one derivatives (**7a**–**7j**) was prepared by a multistep procedure involving nucleophilic substitution, deprotection, and coupling. Commercially available 4-fluorophenol was reacted with tert-butyl 3-((methylsulfonyl)oxy)azetidine-1-carboxylate in the presence of cesium carbonate to afford intermediate chemical 3. Boc deprotection afforded compound 4. Nucleophilic substitution of this intermediate with 4-bromo-6-chloropyridazin-3(2*H*)-one (5) yielded intermediate 6, which subsequently underwent Suzuki–Miyaura coupling with various boronic acids to generate the final derivatives **7a–7j** [14]. See Scheme 1 and 2.

Ten pyridazine derivatives (**7a**–**7j**) were synthesized by substituting the pyridazinone ring at positions 4 and 6. The derivatives contained different C-6 substituents, including electron-donating and electron-withdrawing [15]. The isolated yields for **7a**–**7j** ranged from 12% to 19%, depending on the substituents. The final compounds were obtained as off-white or light-yellow solids and showed good solubility in DMSO and methanol. The formation of the azetidinyl ether linkage was the key step, and the choice of base and solvent significantly influenced the conversion. Cesium carbonate and DMF provided the best performance under the tested conditions. Reaction progress was monitored by TLC using ethyl acetate:hexane and MeOH:dichloromethane solvent systems. All final compounds were purified by column chromatography, and their purities were assessed by LC-MS analysis.

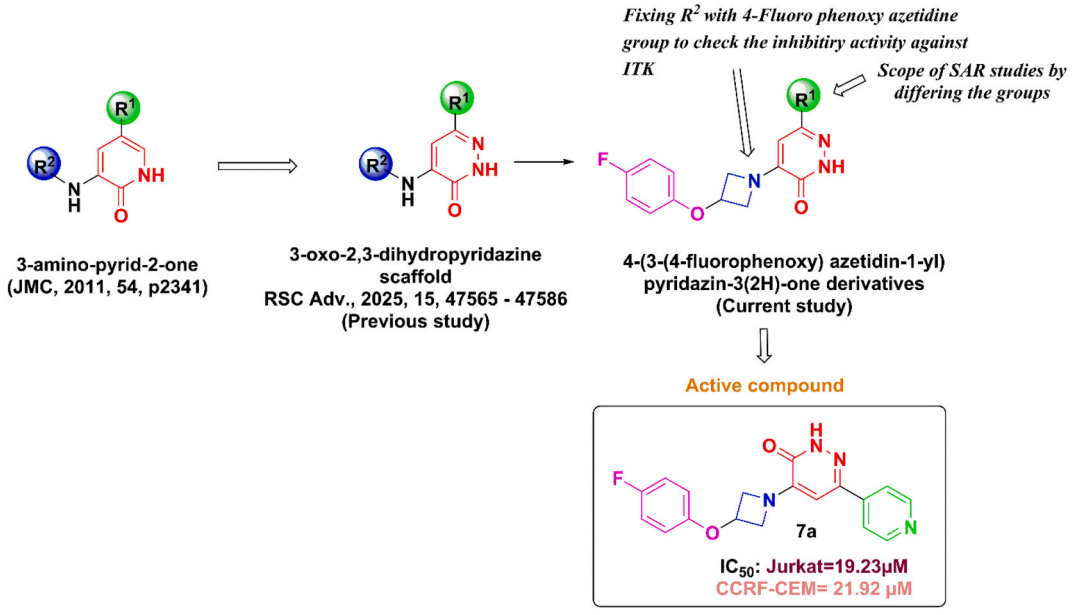
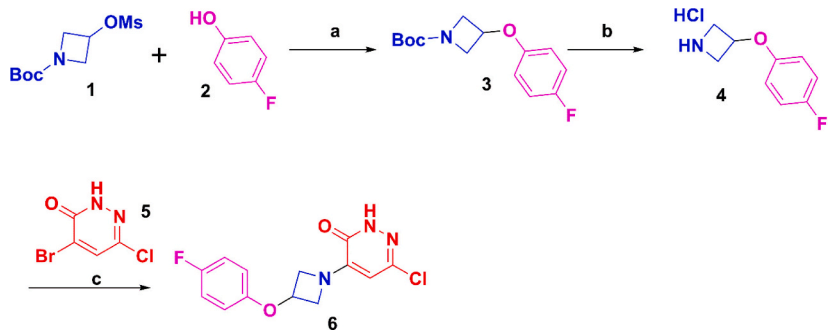
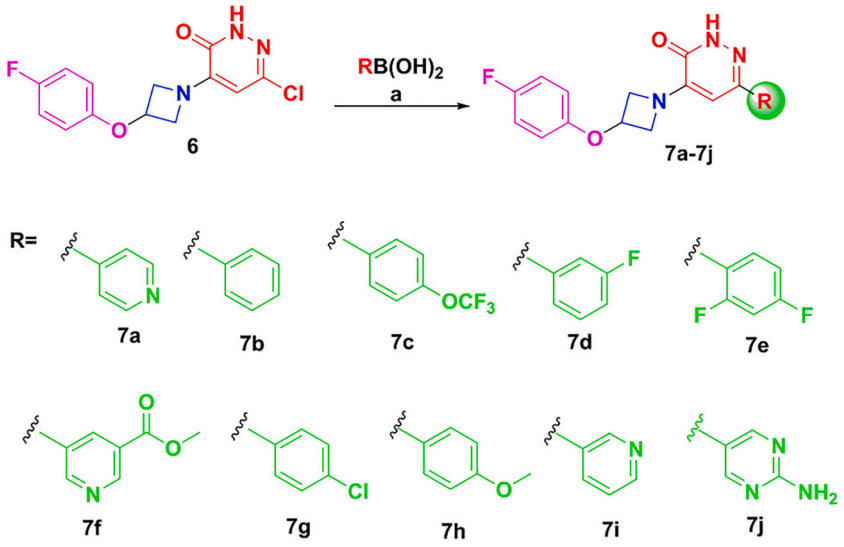



**Fig. 1.** Design progression from reported 3-aminopyrid-2-one ITK ligands and the previously studied 3-oxo-2,3-dihydropyridazine scaffold to the present 4-(3-(4-fluorophenoxy)azetidin-1-yl)pyridazin-3(2*H*)-one derivatives. The fluorophenoxy-azetidinyl unit was incorporated at C-4, while the C-6 substituent was varied across compounds **7a–7j.** The diagram illustrates the chemical design lineage and does not establish ITK inhibition by the current compounds.



**Scheme 1.** Synthesis of compound **6**: **Reaction condition:** (a) $Cs_2CO_3$, DMF, 80 °C, 16 h; (b) 4 M HCl in 1,4-dioxane, 3 h; (c) DIPEA, DMF, RT, 16 h.



**Scheme 2.** Synthesis of compounds **7a** to **7j**: **Reaction condition:** (a) 2 N $Na_2CO_3$, Pd(dppf)$Cl_2$.$CH_2Cl_2$, 1,4-dioxane, 100 °C, 16 h.

Reported LC–MS purities ranged from 90.55% to 99.38%. Compounds **7b** (94.71%), **7 g** (92.0%), and **7j** (90.55%) had purities below 95%. Their cell-viability results are included in the next section for completeness but were excluded from the structure–activity relationship (SAR) analysis.

### 2.2. Evaluation of cytotoxic activity

The effects of the synthesized compounds on cell viability were evaluated after 72 h using an MTS assay, as described previously [16]. Primary interpretation was restricted to compounds with reported LC–MS purity of at least 95%. Among the tested compounds, **7a** exhibited the greatest effect on cell viability, with $IC_{50}$ values of 19.23 ± 1.19 μM in Jurkat cells, 21.92 ± 2.47 μM in CCRF-CEM cells, and 22.59 ± 2.79 μM in Ramos cells (Table 1). These results show that **7a** had a moderate effect on viability in both T- and B-cell leukemia lines; however, the cellular data do not identify the molecular target responsible for this effect. No $IC_{50}$ below 50 μM was observed for **7a** in A549, HCT116, HCT116 TP53$^{-/-}$, U2OS, K562, BJ, or MRC-5 cells under either tested fibroblast seeding condition. Compared with non-

**Table 1**
Cytotoxicity of synthesized 4-(3-(4-fluorophenoxy) azetidin-1-yl) pyridazin-3(2H)-one derivatives (**7a**–**7j**) in human cancer and non-cancer cell lines. $IC_{50}$ values are expressed in μM (Values >50 indicate that an $IC_{50}$ was not reached at the highest concentration tested). LD, low-density fibroblast seeding condition. Data are presented as mean ± SD from ≥6 replicates.

| | ITK/BTK-negative solid-tumor models | | | | ITK-positive T-cell leukemia models | | BTK-positive hematological models | | Non-cancer fibroblast | | | |
|---|---|---|---|---|---|---|---|---|---|---|---|---|
| Compound | *A549* | *HCT116* | *HCT116 TP53$^{-/-}$* | *U2OS* | *CCRF-CEM* | *Jurkat* | *K562* | *Ramos* | *BJ* | *BJ (LD)* | *MRC-5* | *MRC-5 (LD)* |
| 7a | >50 | >50 | >50 | >50 | 21.92 ± 2.47 | 19.23 ± 1.19 | >50 | 22.59 ± 2.79 | >50 | >50 | >50 | >50 |
| 7b | >50 | >50 | >50 | >50 | >50 | >50 | >50 | >50 | >50 | >50 | >50 | >50 |
| 7c | >50 | >50 | >50 | >50 | >50 | >50 | >50 | >50 | >50 | >50 | >50 | >50 |
| 7d | >50 | >50 | >50 | >50 | >50 | >50 | >50 | >50 | >50 | >50 | >50 | >50 |
| 7e | >50 | >50 | >50 | >50 | 41.15 ± 5.01 | >50 | >50 | >50 | >50 | >50 | >50 | >50 |
| 7f | >50 | >50 | >50 | 39.92 ± 5.57 | 30.39 ± 6.83 | >50 | >50 | >50 | >50 | 44.56 ± 2.76 | >50 | >50 |
| 7 g | >50 | >50 | >50 | >50 | 45.39 ± 3.35 | >50 | >50 | >50 | >50 | >50 | >50 | >50 |
| 7 h | >50 | >50 | >50 | >50 | >50 | >50 | >50 | >50 | >50 | >50 | >50 | >50 |
| 7i | >50 | >50 | >50 | >50 | 34.33 ± 3.97 | >50 | >50 | >50 | >50 | >50 | >50 | >50 |
| 7j | >50 | >50 | >50 | 42.27 ± 5.66 | 38.31 ± 4.66 | >50 | >50 | >50 | >50 | >50 | >50 | >50 |

cancer fibroblasts, **7a** showed a > 2.2–2.6-fold increase in cellular activity in Jurkat, CCRF-CEM, and Ramos cells, with no $IC_{50}$ observed in BJ or MRC-5 fibroblasts at concentrations up to 50 μM.

Among the other compounds meeting the purity threshold, **7e** and **7i** showed activity only in CCRF-CEM cells, with $IC_{50}$ values of 41.15 ± 5.01 and 34.33 ± 3.97 μM, respectively. Compound **7f** affected CCRF-CEM, U2OS, and low-density BJ cells, with $IC_{50}$ values of 30.39 ± 6.83, 39.92 ± 5.57, and 44.56 ± 2.76 μM, respectively, indicating no clear cell-line-specific pattern. Compounds **7c**, **7d**, and **7 h** did not reach an $IC_{50}$ within the tested concentration range. Results for **7b**, **7 g**, and **7j** are provided in Table 1 but were excluded from the SAR interpretation because their reported purities were below 95%. Overall, **7a** emerged as the most promising molecule in the series, exhibiting inhibitory activity against both ITK and BTK-expressing leukemia cells.

### 2.3. Biochemical ITK and BTK activity

Compound **7a**, the most consistently active derivative in the cellular assays, and compound **7e**, which showed the most favorable ITK docking score, were selected to assess their direct inhibitory effects on recombinant ITK and BTK. Both compounds were tested at 1, 10, and 20 μM. Ibrutinib, a reference inhibitor of ITK and BTK [7], was tested at the same concentrations (Fig. 3).

Compound **7a** significantly inhibited both kinases at 10 and 20 μM. At 20 μM, ITK and BTK activities were reduced to 58.7 ± 5.2% and 58.5 ± 3.6% of vehicle control, respectively. At 10 μM, ITK and BTK activities were 91.8 ± 1.4% and 87.8 ± 0.6%, respectively. The comparable effects on both kinases demonstrate dual ITK/BTK inhibitory activity.

Compound **7e** did not significantly inhibit either kinase at the tested concentrations. In contrast, ibrutinib significantly inhibited both ITK and BTK at all concentrations, confirming assay responsiveness. Overall, **7a** emerged as the biochemically active compound, exhibiting moderate dual inhibition of ITK and BTK at 20 μM. The favorable docking score of **7e** did not translate into measurable kinase inhibition under the tested conditions. As neither compound produced more than 50% inhibition, $IC_{50}$ values were not calculated.

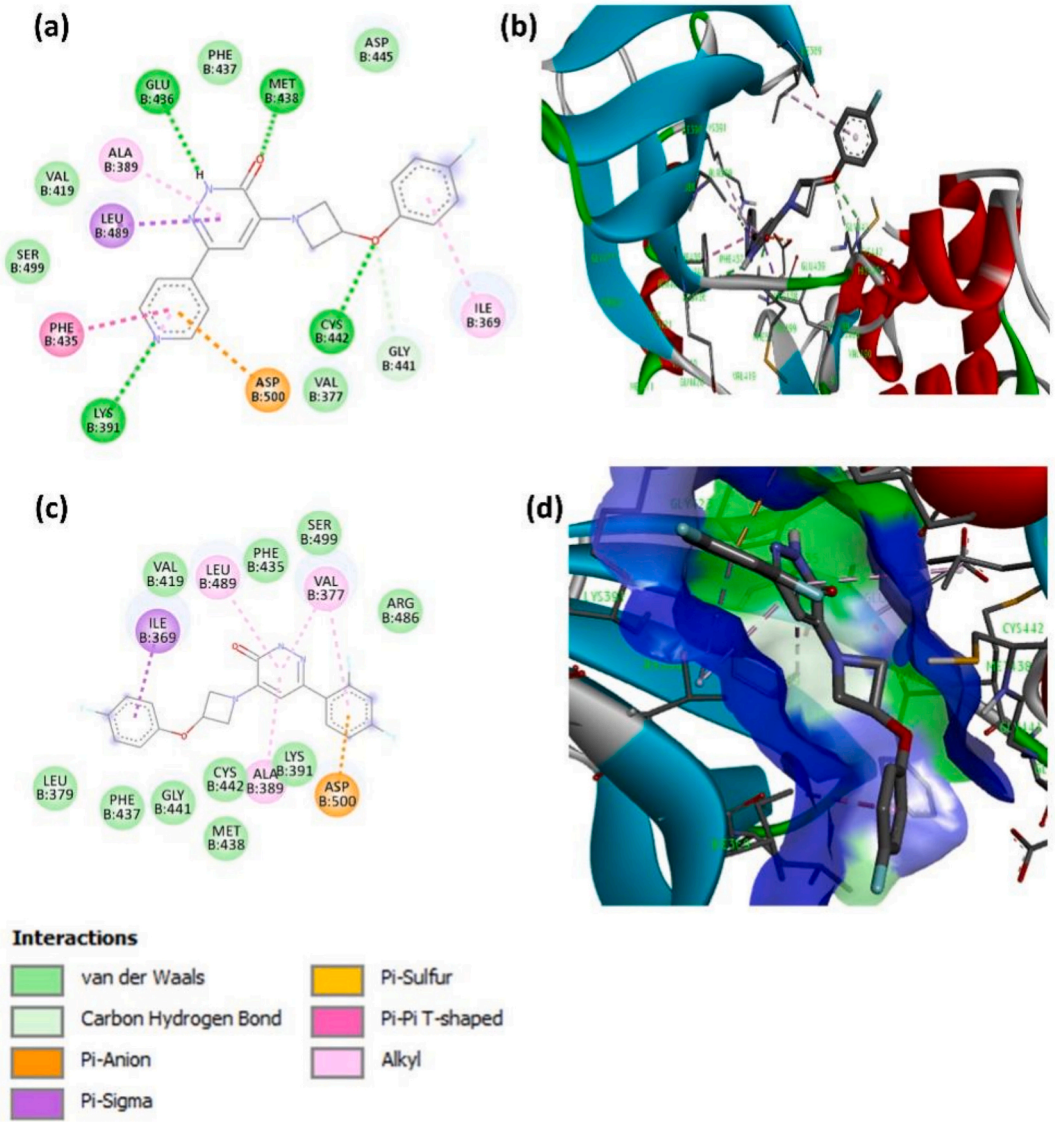



**Fig. 3.** Predicted binding modes of compounds 7a and 7e within the ATP-binding pocket of human ITK (PDB ID: 3QGW). (a) Two-dimensional interaction map and (b) three-dimensional docking pose of 7a; (c) two-dimensional interaction map and (d) three-dimensional docking pose of 7e. The predicted binding mode of 7a included conventional hydrogen bonds with Glu436, Met438, Cys442, and Lys391. No conventional hydrogen bonds were predicted for 7e; its binding mode included alkyl and π-related interactions with Leu489, Val377, Ala389, Ile369, and Asp500. Interaction types are indicated by the color key.

### 2.4. Molecular docking

Molecular docking studies were performed using the human ITK crystal structure (PDB ID: 3QGW) to examine how the synthesized pyridazinone derivatives may interact with the ATP-binding pocket. The docking scores of compounds **7a**–**7j** ranged from −8.5 to −7.5 kcal/mol. Within the series, **7e** had the most favorable predicted docking score (−8.5 kcal/mol), followed by **7a** (−7.8 kcal/mol). Predicted docking scores and protein–ligand interactions for compounds **7a**–**7j**, ibrutinib, and the co-crystallized ligand L7A are provided in Table S1. Additional binding poses and interaction maps are presented in Fig. S1.

The predicted binding mode of **7a** included conventional hydrogen bonds with Glu436, Met438, Cys442, and Lys391. Additional predicted interactions included a π–sigma interaction with Leu489, alkyl interactions with Ala389 and Ile369, a π–π T-shaped interaction with Phe435, and a π–anion interaction with Asp500. No conventional hydrogen bonds were predicted for **7e**; its binding mode included alkyl interactions with Leu489, Val377 and Ala389, a π–sigma interaction with Ile369 and a π–anion interaction with Asp500 (Fig. 2). These findings indicate that both compounds could be accommodated within the predicted ITK ATP-binding pocket through distinct interaction patterns.

## 3. Discussion

This study combined cell-viability profiling, molecular docking, and recombinant kinase assays to evaluate a new series of pyridazinone–azetidine derivatives. Among the compounds included in the primary biological evaluation, **7a** showed the broadest and most consistent cellular activity, particularly in Jurkat, CCRF-CEM, and Ramos cells, while its activity was lower in the other tested cancer and non-cancer models. These findings identify **7a** as the principal cellularly active analog within the present series. Cell-viability results represent phenotypic activity and are therefore considered separately from the biochemical kinase data.

Direct biochemical evaluation demonstrated that **7a** significantly inhibited both ITK and BTK at 10 and 20 μM, with comparable effects on the two kinases. Under the tested conditions, **7a** therefore exhibited moderate dual ITK/BTK inhibitory activity, without evidence of preferential inhibition of either kinase. Because kinase activity remained above 50% throughout the tested concentration range, kinase $IC_{50}$ values were not evaluated. The reference inhibitor ibrutinib inhibited both kinases under the same conditions, supporting the performance of the assays. Thus, the recombinant kinase experiments directly establish the dual biochemical activity of **7a** without attributing its cellular effects specifically to ITK or BTK inhibition.

Molecular docking provided possible binding orientations for the compounds within the ITK ATP-binding pocket. The predicted pose of **7a** included hydrogen-bond, hydrophobic, and π-related interactions that may support its accommodation within the active site and provide structural information for further analog design. However, **7e** produced the most favorable docking score in the series but did not significantly inhibit either ITK or BTK, whereas **7a** showed a less favorable docking score but measurable inhibition of both kinases. The docking-score ranking, therefore, did not predict the experimentally observed kinase activity.

The predicted accommodation of **7e** may be associated with its difluorophenyl substitution, which participated in predicted hydrophobic and π-related contacts within the ITK pocket, consistent with computational observations reported for other ITK ligands [17]. These predicted interactions provide a structural hypothesis for the docking result but do not represent experimentally measured binding affinity. The comparison between **7a** and **7e** demonstrates the complementary roles of the two approaches: docking can suggest possible ligand orientations and interactions, whereas biochemical assays establish kinase-inhibitory activity.

Within the present series, the activity of the 4-pyridyl-substituted compound **7a** suggests that this substituent may favor both cellular and biochemical activity. Because pronounced activity was concentrated in one analog, this should be regarded as an initial structure–activity observation rather than a definitive SAR. Compounds **7b**, **7 g**, and **7j** were retained in the synthetic and analytical reporting but were excluded from the primary biological interpretation and SAR because their reported LC–MS area purities were below 95%.

Overall, the combined findings identify **7a** as the most informative analog in the series, combining cellular activity in selected lymphoid cancer models with experimentally demonstrated dual ITK/BTK inhibition. Its 4-pyridyl substitution and predicted binding orientation provide a focused basis for further optimization of the pyridazinone–azetidine scaffold.

A series of ten 4-(3-(4-fluorophenoxy)azetidin-1-yl)pyridazin-3(2*H*)-one derivatives (**7a**–**7j**) synthesized and evaluated through cell-viability assays, molecular docking, and recombinant kinase assays. Among the synthesized compounds, **7a** demonstrated the most consistent cellular activity, particularly against Jurkat, CCRF-CEM, and Ramos leukemia/lymphoma cell lines. Biochemical evaluation showed that **7a** produced partial inhibition of both recombinant ITK and BTK at 20 μM, with comparable effects on the two kinases and therefore no evidence of preferential ITK inhibition. In contrast, **7e**, despite exhibiting the most favorable predicted ITK docking score, showed no measurable inhibition of either recombinant kinase, highlighting the limitations of relying solely on docking scores to predict biochemical activity. Overall, 7a

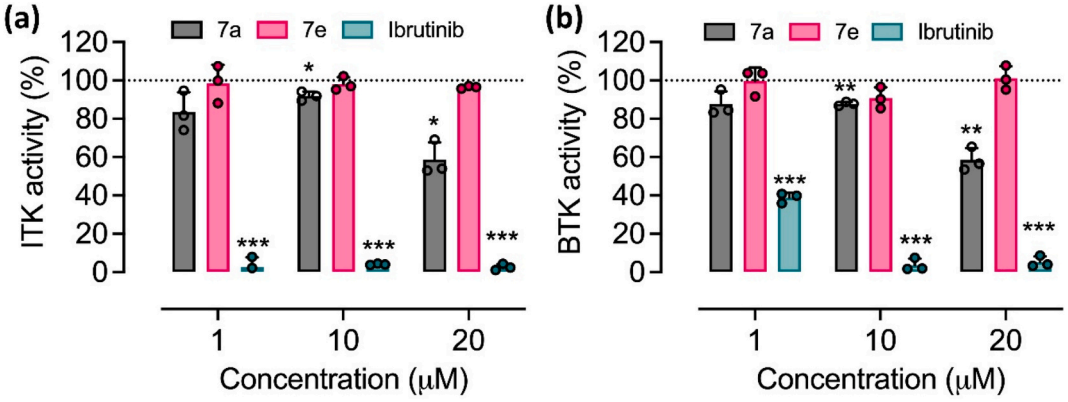



**Fig. 2.** Effects of compounds 7a and 7e on recombinant ITK and BTK activity. (a) ITK and (b) BTK activity following treatment with 7a, 7e, or the reference inhibitor ibrutinib at 1, 10, and 20 μM. Kinase activity was normalized to the DMSO-treated control, set to 100% (indicated by the dotted line). Data are mean ± SEM ($n = 3$). $^{*}P < 0.05$, $^{**}P < 0.01$, and $^{***}P < 0.001$ vs. DMSO-treated control (100%), two-tailed one-sample *t*-test.

represents an experimentally supported starting point for further structure activity relationship studies and optimization of the pyridazinone azetidine scaffold.

## 4. Experimental procedure

### 4.1. Materials and physical measurements

All reagents employed in the experimental work were obtained from standard commercial vendors, namely Sigma-Aldrich (St. Louis, Missouri, USA), BLD Pharmatech Ltd. (Shanghai, China), and Combi-Blocks (San Diego, California, USA). The progress of the reactions was monitored by thin-layer chromatography (TLC) on Supelco TLC aluminum sheets (silica gel 60 F254 MS-grade). Proton ($^{1}$H) and carbon ($^{13}$C) nuclear magnetic resonance (NMR) spectra were recorded on a Bruker Ascend 400 MHz NMR spectrometer (Billerica, MA, USA), with chemical shifts reported in parts per million (ppm) relative to an internal tetramethylsilane (TMS) reference. Signal Multiplicity abbreviations: s (singlet), d (doublet), t (triplet), q (quartet), m (multiplet). Mass spectra were recorded using a Shimadzu system operating in positive and negative ion mode, and the data were processed with the instrument's standard software. Infrared (IR) spectra were recorded on a Shimadzu IR Affinity-1S FT-IR spectrometer, and only the characteristic absorption bands are reported in wavenumbers ($cm^{-1}$).

### 4.2. General procedure for Suzuki coupling reaction

Compounds **7a–7j** were prepared by Suzuki–Miyaura cross-coupling [18] using the following general procedure. A solution of 6-chloro-4-(3-(4-fluorophenoxy)azetidin-1-yl)pyridazin-3(2H)-one **6** (150 mg, 0.507 mmol, 1.0 equiv.) in 1,4-dioxane (10 mL) was stirred, and 2 N $Na_2CO_3$ (3.0 equiv) and pyridin-4-yl boronic acid (1.3 equiv) were added. The mixture was degassed with argon for 5 min, followed by the addition of Pd(dppf)$Cl_2$·$CH_2Cl_2$ (0.1 equiv). The reaction was heated at 100 °C for 16 h. After completion, the mixture was cooled, diluted with ice-cold water (30 mL), and extracted with ethyl acetate (2 × 30 mL). The combined organic layers were washed with brine (20 mL), dried over anhydrous $Na_2SO_4$, filtered, and concentrated under reduced pressure. The crude product was purified by flash chromatography on a Biotage Claricep 12 g silica cartridge using 5–10% MeOH in $CH_2Cl_2$ as eluent to afford the final compound.

### 4.3. Synthesis

#### 4.3.1. Preparation of tert-Butyl 3-(4-fluorophenoxy)azetidine-1-carboxylate (3)

A mixture of 4-fluorophenol 2 (0.89 g, 7.95 mmol, 1.0 equiv) and cesium carbonate (3.6 g, 11.92 mmol, 1.5 equiv) in DMF (20 mL) was stirred, and tert-butyl 3-((methylsulfonyl)oxy)azetidine-1-carboxylate 1 (2.0 g, 7.95 mmol, 1.0 equiv) was added at room temperature. The reaction mixture was heated at 80 °C for 16 h. Upon completion, the mixture was cooled, diluted with ice-cold water (75 mL), and extracted with ethyl acetate (2 × 100 mL). The combined organic extracts were washed with brine, dried over anhydrous $Na_2SO_4$, filtered, and concentrated under reduced pressure. The crude product was purified by flash chromatography on a BUCHI 40 g Claricep silica gel cartridge using 20–30% EtOAc in petroleum ether as the eluent, affording tert-butyl 3-(4-fluorophenoxy)azetidine-1-carboxylate 3 (1.4 g, 66%) as an off-white solid. $^{1}$H NMR (400 MHz, $CDCl_3$): $\delta$ 6.00–6.95 (m, 2H), 6.70–6.66 (m, 2H), 4.82 (s, 1H), 4.29–4.25 (m, 2H), 4.01–3.96 (m, 2H), 1.44 (s, 9H); LC-MS (ES-API): $m/z$ = 212.1 (M-56 + H)+ [19].

#### 4.3.2. Preparation of 3-(4-Fluorophenoxy)azetidine hydrochloride (4)

To a solution of tert-butyl 3-(4-fluorophenoxy)azetidine-1-carboxylate 3 (700 mg, 2.62 mmol, 1.0 equiv) at 0 °C was added 4 M hydrochloric acid in 1,4-dioxane (7 mL) dropwise. The reaction mixture was then heated to room temperature and stirred for 3 h. After completion, the solvent was removed under reduced pressure, and the residue was washed with diethyl ether (2 × 20 mL), filtered, and dried under vacuum to afford 400 mg (75%) of 3-(4-fluorophenoxy)azetidine hydrochloride 4 as an off -white solid. LC-MS (ES-API): $m/z$ = 168.1 (M + H) + .

#### 4.3.3. Preparation of 6-chloro-4-(3-(4-fluorophenoxy)azetidin-1-yl) pyridazin-3(2H)-one (6)

A solution of 3-(4-fluorophenoxy)azetidine hydrochloride 4 (400 mg, 1.964 mmol, 1.0 equiv) in DMF (10 mL) was stirred, and 4-bromo-6-chloropyridazin-3(2H)-one **5** (411 mg, 1.964 mmol, 1.0 equiv) and DIPEA (1.0 mL, 5.862 mmol, 3.0 equiv) were added at 0 °C under a nitrogen atmosphere. The reaction mixture was stirred at room temperature for 16 h, and progress was monitored by TLC. After completion, the mixture was diluted with ice-cold water (10 mL) and extracted with ethyl acetate (2 × 50 mL). The combined organic layers were washed with brine (20 mL), dried over anhydrous $Na_2SO_4$, filtered, and concentrated under reduced pressure. The crude product was purified by flash chromatography on a Biotage Claricep 12 g silica cartridge using 5–10% methanol in $CH_2Cl_2$ as the eluent to afford 6-chloro-4-(3-(4-fluorophenoxy)azetidin-1-yl)pyridazin-3(2H)-one **6** (350 mg, 60%) as a pale yellow solid. LC-MS (ES-API): $m/z$ = 296.24 (M + H)+ [20].

#### 4.3.4. Preparation of 4-(3-(4-fluorophenoxy)azetidin-1-yl)-6-(pyridin-4-yl)pyridazin-3(2H)-one (7a)

The reaction was performed according to the general procedure described above in 5.2. (Yield: 32 mg, 18%, off-white solid). $^{1}$H NMR (400 MHz, DMSO-$d_6$): $\delta$ 12.81 (s, 1H), 8.63 (d, $J$ = 6.0 Hz, 2H), 7.82 (d, $J$ = 6.0 Hz, $J$ = 1.6 Hz, 2H), 7.18–7.13 (m, 2H), 6.92–6.88 (m, 2H), 6.61 (s, 1H), 5.15–5.10 (m, 1H), 4.69 (br s, 2H); 4.17 (br s, 2H); $^{13}$C NMR (400 MHz, DMSO-$d_6$): 158.9, 156.7, 155.7, 152.6, 150.0, 145.0, 143.0, 119.9, 116.2116.0, 115.9, 99.0, 67.2, 59.6; IR: 1649.1 $cm^{-1}$(C═O stretching); LC-MS (ES-API): $m/z$ = 339.11 $(M + H)^{+}$, 99.38% purity by LC-MS; MR: 252–255 °C.

#### 4.3.5. Preparation of 4-(3-(4-fluorophenoxy)azetidin-1-yl)-6-phenylpyridazin-3(2H)-one (7b)

The reaction was performed according to the general procedure described above in 5.2. (Yield: 28 mg, 16%, light brown solid). $^{1}$H NMR (400 MHz, DMSO-$d_6$): $\delta$ 12.60 (s, 1H), 7.82 (d, $J$ = 7.2 Hz, 2H), 7.43–7.39 (m, 3H), 7.18–7.14 (m, 2H),), 6.91–6.90 (m, 2H), 6.50 (s, 1H), 5.11 (br s, 1H), 4.67 (br s, 2H), 4.15 (br s, 2H); $^{13}$C NMR (400 MHz, DMSO-$d_6$): 158.0, 156.5, 155.7, 152.6, 145.4, 144.9, 136.0, 128.6, 128.5, 125.7, 116.2, 116.0, 115.9, 99.7, 67.3, 59.6; IR: 1641.4 $cm^{-1}$(C═O stretching); LC-MS (ES-API): $m/z$ = 338.1 $(M + H)^{+}$, 94.71% purity by LC-MS; MR: 240–243 °C.

#### 4.3.6. Preparation of 4-(3-(4-fluorophenoxy)azetidin-1-yl)-6-(4-(trifluoromethoxy)phenyl)pyridazin-3(2H)-one (7c)

The reaction was performed according to the general procedure described above in 5.2. (Yield: 26 mg, 12%, light brown solid). $^{1}$H NMR (400 MHz, DMSO-$d_6$): $\delta$ 12.66 (s, 1H), 7.95 (dd, $J$ = 6.8 Hz, $J$ = 2.0 Hz, 2H), 7.42 (d, $J$ = 8.0 Hz, 2H), 7.16 (d, $J$ = 8.8 Hz, 2H), 6.92–6.89 (m, 2H), 6.53 (s, 1H), 5.13–5.10 (m, 1H),), 4.81–4.61 (m, 2H), 4.81–4.22 (m, 2H); $^{13}$C NMR (400 MHz, DMSO-$d_6$): 158.1, 156.5, 155.7, 152.6, 149.9, 148.5, 144.9, 144.2, 136.1, 135.3, 127.7, 123.8, 121.32, 121.0, 119.6, 118.7, 116.2, 116.0, 115.9, 99.5, 67.31, 59.6; IR: 1643.98 $cm^{-1}$(C═O stretching); LC-MS (ES-API): $m/z$ = 422.19 $(M + H)^{+}$, 96.31% purity by LC-MS; MR: 178–180 °C.

#### 4.3.7. Preparation of 4-(3-(4-fluorophenoxy)azetidin-1-yl)-6-(3-fluorophenyl)pyridazin-3(2H)-one (7d)

The reaction was performed according to the general procedure described above in 5.2. (Yield: 31 mg, 17%, light brown solid). $^{1}$H NMR (400 MHz, DMSO-$d_6$): $\delta$ 12.60 (s, 1H), 7.68 (d, $J$ = 14.4 Hz, 1H), 7.65 (d,

$J$ = 9.2 Hz, 1H), 7.50–7.44 (m, 1H), 7.22 (t, $J$ = 9.2 Hz, 1H), 7.17 (t, $J$ = 7.6 Hz, 2H), 6.93–6.88 (m, 2H), 6.55 (s, 1H), 5.14–5.04 (br s, 1H), 4.68 (br s, 2H), 4.13 (br s, 2H). $^{13}$C NMR (400 MHz, DMSO-$d_6$): 163.6, 161.2, 158.0, 156.5, 155.7, 152.6, 144.9, 144.2138.5, 138.4, 130.5130.4, 121.7, 116.2116.0, 115.9, 115.4, 115.2, 112.5, 112.3, 99.5,67.2, 59.6; IR: 1643.1 cm$^{-1}$(C═O stretching); LC-MS (ES-API): $m/z$ = 356.2 (M + H)$^+$, 96.38% purity by LC-MS; MR: 235–237 °C.

#### 4.3.8. Preparation of 6-(2,4-difluorophenyl)-4-(3-(4-fluorophenoxy) azetidin-1-yl)pyridazin-3(2H)-one (7e)

The reaction was performed according to the general procedure described above in 5.2. (Yield: 32 mg, 17%, light brown solid). $^1$H NMR (400 MHz, DMSO-$d_6$): $\delta$ 12.72 (s, 1H), 7.70–7.64 (m, 1H), 7.35 (), 7.19–7.11 (m, 3H), 6.91–6.87 (m, 2H), 6.22 (d, $J$ = 1.6 Hz, 1H), 5.11–5.07 (m, 1H), 4.64 (br s, 2H), 4.13 (br s, 2H). $^{13}$C NMR (400 MHz, DMSO-$d_6$): 163.6, 163.5, 161.1, 161.0, 160.8, 160.7, 158.3, 158.2, 158.0, 156.3, 155.7, 152.6, 144.5, 141.9, 131.4, 131.3, 121.4, 121.3, 121.2, 116.2, 116.0, 115.9, 112.0, 111.9, 111.7, 104.8, 104.5, 104.3, 102.1, 67.3, 59.4; IR: 1588.03 cm$^{-1}$(C═O stretching); LC-MS (ES-API): $m/z$ = 374. 21 (M + H)$^+$, 96.34% purity by LC-MS; MR: 161–162 °C.

#### 4.3.9. Preparation of methyl 5-(5-(3-(4-fluorophenoxy)azetidin-1-yl)-6-oxo-1,6-dihydropyridazin-3-yl)nicotinate (7f)

The reaction was performed according to the general procedure described above in 5.2. (Yield:38 mg, 19%, light brown solid). $^1$H NMR (400 MHz, DMSO-$d_6$): $\delta$ 12.80 (s, 1H), 9.27 (d, $J$ = 2.4 Hz, 1H), 9.08 (d, $J$ = 2.0 Hz, 1H), 8.66 (t, $J$ = 2.0 Hz, 1H), 7.16 (t, $J$ = 2.0 Hz, 2H), 6.93–6.89 (m, 2H), 6.69 (s, 1H), 5,14–5.11 (m, 1H), 4.72 (br s, 2H), 4.19 (br s, 2H), 3,92(s, 3H); $^{13}$C NMR (400 MHz, DMSO-$d_6$): 165.09, 158.1, 156.5, 155.7, 152.5, 150.6, 149.6, 145.0, 142.18, 133.3, 131.6, 125.4, 116.2, 116.0, 115.9, 99.0, 67.2, 59.8, 52.5; IR: 1719.15 cm$^{-1}$(C═O stretching); LC-MS (ES-API): $m/z$ = 397.23 (M + H)$^+$, 95.63% purity by LC-MS; MR: 245–247 °C.

#### 4.3.10. Preparation of 6-(4-chlorophenyl)-4-(3-(4-fluorophenoxy) azetidin-1-yl)pyridazin-3(2H)-one (7 g)

The reaction was performed according to the general procedure described above in 5.2. (Yield: 25 mg, 13%, light brown solid). $^1$H NMR (400 MHz, DMSO-$d_6$): $\delta$ 12.65 (br s, 1H), 7.86 (d, $J$ = 8.8 Hz, 2H), 7.49 (d, $J$ = 8.8 Hz, 2H), 7.15 (t, $J$ = 12.0 Hz, 2H), 6.92–6.89 (m, 2H), 6.52 (s, 1H), 5.12–5.10 (m, 1H), 4,67 (br s, 2H), 4.16 (br s, 2H); $^{13}$C NMR (400 MHz, DMSO-$d_6$): 160.4, 158.1, 156.5, 155.7, 152.6, 144.9, 144.3, 138.2, 134.8, 133.4, 128.5, 127.5, 116.2, 116.0, 115.9, 99.4, 67.3, 59.7; IR: 1640.07 cm$^{-1}$(C═O stretching); LC-MS (ES-API): $m/z$ = 372.12 (M + H)$^+$ 92.0% purity by LC-MS; MR: 213–215 °C.

#### 4.3.11. Preparation of 4-(3-(4-fluorophenoxy)azetidin-1-yl)-6-(4-methoxyphenyl)pyridazin-3(2H)-one (7 h)

The reaction was performed according to the general procedure described above in 5.2. (Yield: 31 mg, 16%, light brown solid). $^1$H NMR (500 MHz, DMSO-$d_6$): $\delta$ 12.49 (s, 1H), 7.76 (d, $J$ = 8.5 Hz, 2H), 7.15 (t, $J$ = 9.0 Hz, 2H), 6.91–6.89 (m, 2H), 6.46 (s, 1H), 5.10 (br s, 1H), 4.66 (br s, 2H), 4.13 (br s, 2H), 3.79 (s, 3H); $^{13}$C NMR (400 MHz, DMSO-$d_6$): 159.7, 158.0, 156.4, 155.7, 152.6, 145.2, 144.9, 128.5, 127.0, 116.2, 116.0, 115.9, 113.8, 99.5, 67.3, 59.5, 55.1; IR: 1651.5 cm$^{-1}$(C═O stretching); LC-MS (ES-API): $m/z$ = 368.4 (M + H)$^+$, 98.17% purity by LC-MS; MR: 238–240 °C.

#### 4.3.12. Preparation of 4-(3-(4-fluorophenoxy)azetidin-1-yl)-6-(pyridin-3-yl)pyridazin-3(2H)-one (7i)

The reaction was performed according to the general procedure described above in 5.2. (Yield: 23 mg, 13%, a light brown solid). $^1$H NMR (400 MHz, DMSO-$d_6$): $\delta$ 12.72 (s, 1H), 9.03 (d, $J$ = 2.0 Hz, 1H), 8.19 (d, $J$ = 6.0 Hz, 1H), 8.58 (dd, $J$ = 4.8 Hz, $J$ = 1.2 Hz, 1H), 7.48–7.44 (m, 1H), 7.15 (t, $J$ = 11.2 Hz, 2H), 6.92–6.89 (m, 2H), 6.58 (s, 1H), 5.13–5.10 (m, 1H), 4.69 (br s, 2H), 4.17 (br s, 2H); $^{13}$C NMR (400 MHz, DMSO-$d_6$): 158.0, 156.5, 155.7, 152.5, 149.5, 146.9, 145.0, 143.3, 133.1, 131.6, 123.5, 116.2116.0, 115.9, 99.3, 67.3, 59.6; IR: 1642.1 cm$^{-1}$(C═O stretching); LC-MS (ES-API): $m/z$ = 339.2 (M + H)$^+$,99.34% purity by LC-MS; MR: 242–244 °C.

#### 4.3.13. Preparation of 6-(2-aminopyrimidin-5-yl)-4-(3-(4-fluorophenoxy) azetidin-1-yl)pyridazin-3(2H)-one (7j)

The reaction was performed according to the general procedure described above in 5.2. (Yield: 22 mg, 12%, light brown solid). $^1$H NMR (400 MHz, DMSO-$d_6$): $\delta$ 12.51 (s, 1H), 8.67 (d, $J$ = 7.2 Hz, 2H), 7.15 (t, $J$ = 12.0 Hz, 2H), 6.92–6.88 (m, 4H), 6.45 (s, 1H), 5.10–5.09 (m, 1H), 4.65 (br s, 2H), 4.13 (br s, 2H); $^{13}$C NMR (400 MHz, DMSO-$d_6$): 163.3, 158.09, 157.97, 156.42, 155.7, 155.51, 152.6, 145.0, 142.3, 118.4, 116.2, 116.0, 115.9, 110.0, 98.6, 67.3, 59.5; IR: 1595.5 cm$^{-1}$(C═O stretching); LC-MS (ES-API): $m/z$ = 355.2 (M + H)$^+$, 90.55% purity by LC-MS; MR: 233–235 °C.

### 4.4. Cytotoxicity assay

All cell lines were obtained from ATCC (Middlesex, UK) or DSMZ (Braunschweig, Germany). Cultures were maintained at 37 °C in a humidified incubator with 5% $CO_2$ in the recommended growth media supplemented with 10% fetal calf serum (Gibco), 1× Penicillin–Streptomycin (Diagnovum), 2 mM L-glutamine (Gibco), 1 mM sodium bicarbonate (Gibco), 1 mM sodium pyruvate (Gibco), and 20 mM HEPES (Gibco). Cells were routinely authenticated by STR profiling [21] and tested biweekly for mycoplasma contamination using established laboratory procedures [22]. Cytotoxic activity of the synthesized pyridazinone derivatives was measured using the MTS assay (CellTiter 96® Aqueous One Solution, Promega), as described previously. Cells were exposed to compounds for 72 h prior to the addition of the MTS reagent, and absorbance was used to quantify viable cells. The cytotoxicity panel included a diverse set of human cancer and non-cancer cell lines representing different tissue origins.

The cancer-cell panel comprised A549 lung adenocarcinoma cells, HCT116 colorectal carcinoma cells, and their isogenic HCT116 TP53$^{-/-}$ derivative, U2OS osteosarcoma cells, K562 chronic myeloid leukemia cells, Ramos Burkitt lymphoma cells, Jurkat T-cell leukemia cells, and CCRF-CEM T-lymphoblastic leukemia cells. Jurkat and CCRF-CEM cells are reported to express ITK, whereas Ramos and K562 cells express BTK [16]. BJ foreskin fibroblasts and MRC-5 lung fibroblasts were included as non-cancer controls and evaluated at standard and low seeding densities.

All assays were performed on an automated high-throughput screening platform (HighResBio, Boston, MA, USA) using our validated in-house protocol. Dose response curves and $IC_{50}$ values were obtained using Dotmatics (San Diego, CA, USA), and data were archived in the MedChemBio database (www.medchembio.imtm.cz).

### 4.5. Molecular docking

The binding modes of compounds **7a–7j** into the ATP-binding pocket of human interleukin-2-inducible T-cell kinase (ITK) were predicted using molecular docking. The crystal structure of ITK with ligand L7A was obtained from the Protein Data Bank (PDB ID: 3QGW). The co-crystallized ligand L7A and non-essential heteroatoms were removed during receptor preparation. The protein was prepared in UCSF Chimera by adding missing hydrogen atoms, optimizing hydrogen-bonding networks and minimizing steric clashes. The L7A was then individually re-docked to test the docking protocol and ibrutinib was used as another reference ligand.

Docking simulations were carried out using AutoDock Vina integrated with UCSF Chimera with the preparation of the receptor and ligand. The docking grid box was centered on the experimentally determined ATP-binding site occupied by L7A with dimensions 21 × 21 × 21 Å and center coordinates X = 21, Y = −74 and Z = 24.2 Å.

The redocking protocol was able to reproduce the crystallographic binding pose of L7A with an RMSD of 1.64 Å, thus validating the reliability of the docking protocol. The structure–activity relationships were examined by studying the binding energies and interactions of hydrogen-bonds of compounds **7a–7j**, ibrutinib and L7A [23,24].

### 4.6. *In vitro biochemical kinase assay*

Recombinant ITK and BTK activities were measured using the ITK Kinase Assay Kit (BPS Bioscience, Cat. No. 78429) and the BTK Kinase Enzyme System (Promega, Cat. No. V2941), respectively, using a procedure adapted from [5]. The enzymes were diluted to 5 ng/μL in their respective 1× kinase reaction buffers. The BTK reaction buffer was additionally supplemented with 50 μM DTT and 2 mM $MnCl_2$.

Compounds **7a** and **7e**, together with the reference inhibitor ibrutinib, were evaluated at 1, 10, and 20 μM in white opaque 384-well plates (Revvity, Part No. 6057480). The final DMSO concentration was 0.25%. DMSO-treated wells served as vehicle controls, while no-enzyme wells, in which the enzyme was replaced with the corresponding reaction buffer, were used to determine background signal.

ADP production was quantified using the ADP-Glo™ Kinase Assay (Promega, Cat. No. V9101) according to the manufacturer's instructions. Luminescence was measured as counts per second using an EnSpire Multimode Plate Reader (PerkinElmer, Waltham, MA, USA), with an integration time of 1 s per well and a measurement height of 0.1 mm. After background subtraction, kinase activity was expressed relative to the DMSO-treated control, which was set to 100%.

Statistical analyses were performed using GraphPad Prism version 11.0.2 (GraphPad Software, Boston, MA, USA). Data are presented as mean ± SEM from three independent replicates. Each treatment was compared with the theoretical value of 100% using a two-tailed one-sample *t*-test, with $P < 0.05$ considered statistically significant.

## CRediT authorship contribution statement

**Sudhakar Tangallapalli:** Writing – original draft, Software, Methodology, Investigation. **Rambabu Gundla:** Supervision, Project administration, Conceptualization. **Kalyani Paidikondala:** Data curation. **Naveen Kumar Rampeesa:** Software, Investigation, Data curation. **Sreenivasa Reddy Anugu:** Resources, Formal analysis. **Soňa Gurská:** Methodology, Investigation. **Petr Džubák:** Resources, Funding acquisition. **Marián Hajdúch:** Resources, Funding acquisition. **Viswanath Das:** Supervision, Methodology, Investigation, Funding acquisition. **Naresh Kumar Katari:** Visualization, Formal analysis.

## Compliance with ethical standards

This study used only established human cell lines and involved no human participants or animals. All work was conducted in accordance with institutional biosafety and good laboratory practice guidelines.

## Declaration of competing interest

The authors declare that they have no known competing financial interests or personal relationships that could have appeared to influence the work reported in this paper.

## Acknowledgements

RG acknowledges GITAM for financial assistance and the facility. GR, RN, and RG thank Aragen Lifesciences Pvt. Ltd., Hyderabad, India, for providing computational resources for the synthesis and characterization of all compounds by NMR, LC-MS, and FT-IR. All biological part of the study was supported in parts by the infrastructural projects (CZ-OPENSCREEN – LM2023052; EATRIS-CZ – LM2023053, BBMRI – LM2023033, and Czech-BioImaging - LM2023050, LM2018129), the projects National Institute for Cancer Research (Program EXCELES, ID Project No. LX22NPO5102, Funded by the European Union - Next Generation EU), project SALVAGE (registration number: CZ.02.01.01/00/22_008/0004644, supported by OP JAK, with co-financing from the EU and the State Budget), all funded by the Ministry of Education, Youth and Sports of the Czech Republic, and the Project TN02000109 (Personalized Medicine: From Translational Research into Biomedical Applications) co-financed with the state support of the Technology Agency of the Czech Republic as part of the National Centers of Competence Program.

## Appendix A. Supplementary data

Supplementary data to this article can be found online at https://doi.org/10.1016/j.rechem.2026.104057.

## Data availability

All data supporting the findings of this study are provided in the article or its Supplementary Information. Compound cytotoxicity data are archived in the IMTM Dotmatics database and the MedChemBio Portal (www.medchembio.imtm.cz) and are available from the corresponding author (*V.* Das) upon reasonable request.

## References

[1] K.S. Lechner, M.F. Neurath, B. Weigmann, Role of the IL-2 inducible tyrosine kinase ITK and its inhibitors in disease pathogenesis, J. Mol. Med. 98 (2020) 1385–1395, https://doi.org/10.1007/s00109-020-01958-z.
[2] Y. Bogin, C. Ainey, D. Beach, D. Yablonski, SLP-76 mediates and maintains activation of the Tec family kinase ITK via the T cell antigen receptor-induced association between SLP-76 and ITK, Proc. Natl. Acad. Sci. USA 104 (2007) 6638–6643, https://doi.org/10.1073/pnas.0609771104.
[3] Weeks S, Harris R, Karimi M. Targeting ITK signaling for T cell-mediated diseases. iScience 2021 24(8):102842. doi: https://doi.org/10.1016/j.isci.2021.102842. (PMID: 34368657; PMCID: PMC8326193).
[4] Z. Fu, Z. Huang, H. Xu, Q. Liu, J. Li, K. Song, Y. Deng, Y. Tao, H. Zhang, P. Wang, H. Li, Y. Sheng, A. Zhou, L. Han, Y. Fu, C. Wang, S.K. Choudhary, K. Ye, G. Veggiani, Z. Li, A. August, W. Huang, Q. Shan, H. Peng, IL-2–inducible T cell kinase deficiency sustains chimeric antigen receptor T cell therapy against tumor cells, J. Clin. Invest. 135 (2025) e178558, https://doi.org/10.1172/JCI178558.
[5] S.Y. Ewieda, E.M. Ahmed, P.A. Halim, et al., Discovery of novel pyridazinone derivatives as EGFRWT/EGFRT790M kinase inhibitors; design, synthesis, antitumor evaluation, and molecular dynamic simulations, Bioorg. Chem. 170 (2026) 109486, https://doi.org/10.1016/j.bioorg.2026.109486.
[6] M.T.M. Nemr, Y.A.A.M. Elshaier, S.Y. Ewieda, M.A. Abdelaziz, Pharmaceutical applications of cyclopropyl containing scaffolds: a review on recent updates, future, Med. Chem. 18 (2026) 79–88, https://doi.org/10.1080/17568919.2025.2594969.
[7] J.A. Dubovsky, K.A. Beckwith, G. Natarajan, J.A. Woyach, S. Jaglowski, Y. Zhong, J.D. Hessler, T.-M. Liu, B.Y. Chang, K.M. Larkin, M.R. Stefanovski, D.L. Chappell, F. W. Frissora, L.L. Smith, K.A. Smucker, J.M. Flynn, J.A. Jones, L.A. Andritsos, K. Maddocks, A.M. Lehman, R. Furman, J. Sharman, A. Mishra, M.A. Caligiuri, A. R. Satoskar, J.J. Buggy, N. Muthusamy, A.J. Johnson, J.C. Byrd, Ibrutinib is an irreversible molecular inhibitor of ITK driving a Th1-selective pressure in T lymphocytes, Blood 122 (2013) 2539–2549, https://doi.org/10.1182/blood-2013-06-507947.
[8] X. Zhang, X. Sheng, J. Shen, S. Zhang, W. Sun, C. Shen, et al., Discovery and evaluation of pyrazolo[3,4-d]pyridazinone as a potent and orally active irreversible BTK inhibitor, ACS Med. Chem. Lett. 11 (2020) 1863–1868, https://doi.org/10.1021/acsmedchemlett.9b00395.
[9] W.B. Young, J. Barbosa, P. Blomgren, M.C. Bremer, J.J. Crawford, D. Dambach, C. Eigenbrot, S. Gallion, A.R. Johnson, J.E. Kropf, S.H. Lee, L. Liu, J.W. Lubach, J. Macaluso, P. Maciejewski, S.A. Mitchell, D.F. Ortwine, J. Di Paolo, K. Reif, H. Scheerens, A. Schmitt, X. Wang, H. Wong, J.M. Xiong, J. Xu, C. Yu, Z. Zhao, K. S. Currie, Discovery of highly potent and selective Bruton's tyrosine kinase inhibitors: pyridazinone analogs with improved metabolic stability, Bioorg. Med. Chem. Lett. 26 (2016) 575–579, https://doi.org/10.1016/j.bmcl.2015.11.076.
[10] D. Zhang, J. Zhao, G. Xu, Y. Wang, Y. Li, H. Ren, J. Geng, Y. Du, C. Zhang, S. Yang, D. Liu, J. Gao, Y. Xiong, H. Zhang, W. Li, W. Wang, D. Wang, B. Li, X. He, C. Ma, Y. Jiang, Q. Ding, Discovery of imidazo[1,2-b]pyridazine derivatives as potent and highly selective irreversible Bruton's tyrosine kinase (BTK) inhibitors, J. Med. Chem. 68 (2025) 10897–10929, https://doi.org/10.1021/acs.jmedchem.4c03083.
[11] N.A. Meanwell, The pyridazine heterocycle in molecular recognition and drug discovery, Med. Chem. Res. 32 (2023) 1853–1921, https://doi.org/10.1007/s00044-023-03035-9.
[12] S.Y. Ewieda, E.M. Ahmed, N.A. Gohar, S.G. Ibrahim, M.A. Essa, M.T.M. Nemr, Design, synthesis, and antitumor evaluation of new pyridazinone scaffolds as dual

EGFR/VEGFR-2 kinase inhibitors and apoptotic cells inducers, Bioorg. Chem. 166 (2025) 109157, https://doi.org/10.1016/j.bioorg.2025.109157.
[13] S. Tangallapalli, R. Gundla, K. Paidikondala, S. Gurská, N.K. Rampeesa, S. R. Anugu, P. Džubák, M. Hajdúch, V. Das, N.K. Katari, Design, synthesis, and biological evaluation of novel 3-oxo-2,3-dihydropyridazine derivatives as interleukin-2-inducible T-cell kinase (ITK) inhibitors, RSC Adv. 15 (2025) 47565–47586, https://doi.org/10.1039/D5RA06565H.
[14] H. Boufroura, B. Large, T. Bsaibess, S. Perato, V. Terrasson, A. Gaucher, D. Prim, Aziridine- and azetidine–Pd catalytic combinations: synthesis and evaluation of the ligand ring size impact on Suzuki–Miyaura reaction issues, Catalysts 7 (2017) 27, https://doi.org/10.3390/catal7010027.
[15] S. Pathak, V. Sharma, N. Agrawal, S. Sharma, Pyridazinone: current progress in synthesis of its derivatives and biological activity, Med. Chem. 21 (2025) 822–842, https://doi.org/10.2174/0115734064363384241217115624.
[16] C.P. Koraboina, V.C. Maddipati, N. Annadurai, S. Gurská, P. Džubák, M. Hajdúch, V. Das, R. Gundla, Synthesis and biological evaluation of oxindole sulfonamide derivatives as Bruton's tyrosine kinase inhibitors, ChemMedChem 19 (2024) e202300511, https://doi.org/10.1002/cmdc.202300511.
[17] S. Ahmed, A. Choudhury, M.U. Saeed, T. Mohammad, A. Hussain, M.F. Alajmi, D. K. Yadav, A. Shamsi, M.I. Hassan, Identification of potential inhibitors of interleukin-2-inducible T-cell kinase: insights from docking, molecular dynamics, MMPBSA and free energy landscape studies, Amino Acids 57 (1-15) (2025), https://doi.org/10.1007/s00726-025-03457-2.
[18] J.W.B. Fyfe, N.J. Fazakerley, A.J.B. Watson, Chemoselective Suzuki–Miyaura cross-coupling via kinetic transmetallation, Angew. Chem. Int. Ed. 56 (2017) 1249–1253.
[19] Preparation of triazinone compounds as T-type calcium channel inhibitors, WO2013147183 A1, 2013.
[20] Preparation of pyridazinones and their uses as BTK inhibitors, WO2010056875 A1, 2010.
[21] J. Stránská, STR profiling for cell line authentication, in: K. Agrawal, J. Bouchal, V. Das, J. Drábek, P. Džubák, M. Hajdúch, K. Koberna, A. Ligasová, M. Mistrík, J. B. de Sanctis, J. Srovnal (Eds.), Laboratory Techniques in Cellular and Molecular Medicine, 1st edn, Palacký University Olomouc, Olomouc, 2022, pp. 29–36, https://doi.org/10.5507/lf.22.24460499.
[22] R. Buriánová, J. Kotulová, Detection of mycoplasma contamination in cell lines by PCR, in: K. Agrawal, J. Bouchal, V. Das, J. Drábek, P. Džubák, M. Hajdúch, K. Koberna, A. Ligasová, M. Mistrík, J.B. de Sanctis, J. Srovnal (Eds.), Laboratory Techniques in Cellular and Molecular Medicine, Palacký University Olomouc, Olomouc, 2022, pp. 37–42, https://doi.org/10.5507/lf.22.24460499.
[23] E.F. Pettersen, T.D. Goddard, C.C. Huang, G.S. Couch, D.M. Greenblatt, E.C. Meng, T.E. Ferrin, UCSF chimera a visualization system for exploratory research and analysis, J. Comput. Chem. 25 (2004) 1605–1612, https://doi.org/10.1002/jcc.20084.
[24] O. Trott, A.J. Olson, AutoDock Vina: improving the speed and accuracy of docking with a new scoring function, efficient optimization, and multithreading, J. Comput. Chem. 31 (2010) 455–461, https://doi.org/10.1002/jcc.21334.